Towards a catheter-based impedimetric sensor for the assessment of intestinal histamine levels in IBS patients

Biosensors and Bioelectronics 158 (2020) 112152

Contents lists available at ScienceDirect

Biosensors and Bioelectronics

journal homepage: http://www.elsevier.com/locate/bios

Towards a catheter-based impedimetric sensor for the assessment of intestinal histamine levels in IBS patients

Gideon Wackers [a,*,1], Tristan Putzeys [a,b,1], Marloes Peeters [c], Lori Van de Cauter [a], Peter Cornelis [a], Michael Wübbenhorst [a], Jan Tack [d], Freddy Troost [e], Nicolas Verhaert [b], Theodor Doll [f], Patrick Wagner [a]

[a] KU Leuven, Laboratory for Soft Matter and Biophysics, Celestijnenlaan 200 D, B-3001, Leuven, Belgium
[b] KU Leuven, Research Group Experimental Oto-rhino-laryngology, O&N II, Herestraat 49, B-3001, Leuven, Belgium
[c] Newcastle University, School of Engineering, Newcastle NE1 7RU, United Kingdom
[d] KU Leuven, Translational Research in Gastrointestinal Disorders, O&N I, Herestraat 49, B-3001, Leuven, Belgium
[e] Food Innovation and Health, Centre for Healthy Eating and Food Innovation, Maastricht University, NUTRIM School of Nutrition and Translational Research in Metabolism, Universiteitssingel 40, NL-6229 ER, Maastricht, the Netherlands
[f] Hannover Medical School, Institute of AudioNeuroTechnology VIANNA, Stadtfelddamm 34, D-30625, Hannover, Germany

ARTICLE INFO

Keywords:
Biomimetic sensors
Impedance spectroscopy
Diagnostic methods
Molecularly imprinted polymers
Irritable bowel syndrome

ABSTRACT

In this work, we report on the development of a catheter-based sensor designed for measuring the concentration of histamine in the human duodenum. Certain gut disorders, such as the irritable bowel syndrome (IBS), are associated with elevated levels of intestinal histamine due to chronic immune activation. As it is still impossible to determine histamine concentrations *in vivo*, a nasointestinal catheter with histamine-sensing capabilities has the potential to become a valuable diagnostic instrument. Regarding the sensing principle, we selected impedance spectroscopy using voltages that are compatible with intra-body applications with molecularly imprinted polymers (MIPs) as recognition elements. MIPs are synthetic receptors that offer the advantages of robustness, high specificity and selectivity for histamine as a target. In this specific case, the MIPs were synthesized from acrylic acid monomers, which guarantees a uniform binding capacity within the pH range of intestinal fluid. We have validated the catheter sensor on human intestinal liquids spiked with histamine in a testing setup that mimics the environment inside the duodenum. The dose-response curves show an analytical range between 5 and 200 nM of histamine, corresponding to physiologically normal conditions while higher concentrations correlate with disease. The key output signal of the sensor is the resistive component of the MIP-functionalized titanium electrodes as derived from the equivalent-circuit modelling of full-range impedance spectra. Future applications could be catheters tailored to cardiovascular, urological, gastrointestinal, and neurovascular applications. This, in combination with the versatility of the MIPs, will make this sensor platform a versatile diagnostic tool.

1. Introduction

In this article, we report on the development of a catheter-based, biomimetic sensor that is able to quantitatively detect histamine in the human duodenum. This is motivated by the fact that elevated histamine levels in the small intestine are a potential biomarker for at least a subset of patients with irritable bowel syndrome IBS (Barbara et al., 2004; Belon et al., 2004; Canavan et al., 2014; Lobo et al., 2017; Wood, 2006; Wouters et al., 2016). IBS is a widespread gastrointestinal disorder with a global prevalence of 11%. However, there are considerable age-, sex-, and region-dependent deviations from this average percentage (Canavan et al., 2014). The diagnosis is mainly symptom based according to the so-called Rome IV criteria (Schmulson and Drossman, 2018). Therapies include dietary adjustments, central neuromodulators, such as tricyclic antidepressants, and herbal medicines, such as peppermint oil (Drossman et al., 2018; Tan et al., 2019). Although IBS has no impact on mortality, it severely compromises the quality of life and also has a high negative economic impact. Recent studies have implicated mast cells

* Corresponding author.
E-mail address: PatrickHermann.Wagner@kuleuven.be (G. Wackers).
[1] Both authors contributed equally.

https://doi.org/10.1016/j.bios.2020.112152
Received 30 January 2020; Received in revised form 9 March 2020; Accepted 12 March 2020
Available online 20 March 2020

and the histamine they release as potential targets for IBS therapy (Lobo et al., 2017; Wouters et al., 2016).

In this sense, we consider the histamine-sensitive catheter as a prospective diagnostic tool, allowing to confirm which patients with IBS-like symptoms (e.g. abdominal pain and altered stool patterns) do indeed have elevated histamine levels due to chronic immune activation with a key role for mast cells (Barbara et al., 2014; Lobo et al., 2017; Wouters et al., 2016). In these patients, triggers such as ingestion of certain food or stress, can cause mast-cell degranulation with histamine release in the duodenum (Fritscher-Ravens et al., 2019). A catheter that measures directly in this environment allows to correlate a stimulus with the provoked histamine release much more precisely than e.g. histamine measurements on stool. The result of such test can also facilitate selecting the most appropriate therapy by adding quantitative information to the "typical" symptoms, which are often subjective and inconclusive. Moreover, it was recently discovered that histamine receptor agonists and mast cell blockers, used to treat allergies, can also reduce the visceral hypersensitivity, immune activation and symptoms in IBS patients (Lobo et al., 2017; Wouters et al., 2016). This underpins the correlation between mast cell activation, increased levels of histamine, and the rather complex spectrum of symptoms and manifestations in IBS. Interestingly, there is the "PillCam" device (a wireless camera packaged as a capsule), which is able to visualize and inspect the interior of the entire intestines (Adler et al., 2011; Pennazio et al., 2015, Van Gossum, 2014). However, this device has no chemical/biological sensing functionality and, because it advances through the intestinal tract due to peristaltic bowel movements, it cannot be used to monitor molecular-biomarker concentrations at a certain location, such as the duodenum, during longer periods.

In biosensor development, it is already a long-time endeavor to create implantable sensors which perform their analytical task *in vivo*, see for instance the review articles by Frost and Meyerhoff (2006), Wilson and Gifford (2005), and by Pickup et al. (2005). Biocompatibility issues were initially a major hurdle, but in case of diabetes management, there was considerable progress on subcutaneously implanted enzyme electrodes for glucose detection. After a long development phase, which started already 30 years ago (Bindra et al., 1991), these needle-shaped electrodes are now well established and need replacement only once every two weeks. To reduce invasiveness even further, there are still ongoing efforts to perform bioanalysis, not limited to glucose, on easily accessible body fluids. This includes measurements on tears with sensors that can be integrated with contact lenses (Yao et al., 2011), on sweat on the epidermis with wearable- or tattoo-type sensors (McCaul et al., 2017; Bandodkar et al., 2014), and on saliva with intra-oral devices (Kim et al., 2015). On the other end of the "invasiveness scale", there are sensors under development aiming at analyzing brain fluid, mainly with respect to neurotransmitters (Frey et al., 2010; Tseng and Monbouquette, 2012), and a review by Kotanen et al. (2012) summarizes the challenges to be overcome before human applications may become feasible.

For our sensing application of histamine release in the intestines, a chronic implant is neither necessary nor technically or physiologically feasible. Strictly speaking, the lumen of the intestines is not *"in vivo"* as no epithelial barriers need to be passed, but the complexity of getting the sensor to the measurement location is clearly higher than measuring e.g. sweat on the epidermis. Therefore, we opted for a catheter-based approach that will eventually enable measurements during several hours (to monitor stimulated histamine release) while being retractable at any time. There are only very few reports on catheter-based bio- and chemosensors in literature and, to best of our knowledge, none of them reached the pre-clinical testing phase on humans yet. Examples include a catheter intended for glucose- and oxygen monitoring in the brain (Li et al., 2009), a foil-type urea sensor that can be coiled up for placing it in a catheter tube (Mamleyev et al., 2019), and a flexible temperature-, flow rate- and glucose sensor meant for insertion in veins (Li et al., 2008). Major progression was made by Loyez et al. (2019) who recently reported on a fiber-optical sensor for lung-cancer biomarkers; the sensor response was validated on human lung tissue and the device was inserted into the lung of a narcotized pig using a bronchoscope. Given the fact that catheters and endoscopes are extremely well developed, see e.g. (Molinnus et al., 2018) for an example on the kidney, one can anticipate that bio-chemical sensors can become a versatile "add-on" that augments the diagnostic capabilities of these widely used instruments.

Regarding the detection principle, we selected impedance spectroscopy in its non-Faradaic form, i.e. without redox mediators, to avoid introducing additional chemicals into the intestine. Impedimetric sensing can be implemented inside a catheter by using wire-type electrodes instead of the more common planar electrodes. Other sensing principles, such as microgravimetry, are hard to miniaturize to fit inside the inner volume of a catheter while heat-transfer measurements, see e.g. (Wackers et al., 2014; van Grinsven et al., 2014), cannot operate in an environment with a homogeneous temperature distribution (body temperature of 37 °C). Concerning the receptors, the main requirement is robustness in a broad pH range because intestinal fluid can vary between pH 5.4 and pH 7.5, depending on the diet and possible leaks of stomach acid into the duodenum (Dressman et al., 1990; Worning and Müllertz, 1966). Also, regeneration capability can be seen as a benefit when aiming at repetitive measurements during several hours with the catheter in place. Antibodies, such as those that are used in ELISA tests for histamine (Aygün et al., 1999; Muscarella et al., 2005), do not fulfill these criteria while histamine-selective aptamers were developed only very recently (Mairal Lerga et al., 2019). Molecularly imprinted polymers (MIPs) for histamine are, however, in a well developed state and besides their robustness and regeneration capacity, their synthesis is straightforward and low cost (Horemans et al., 2010; Mattson et al., 2017; Mattsson et al., 2018; Peeters et al., 2014; Torres et al., 2012; Ramakers et al., 2019 Ratautaite et al., 2014). Specifically, we will utilize powders of acrylic-acid MIPs as electrode coatings due to their proven selectivity, uniform binding affinity for histamine fro5 to pH 9, and earlier successful use for histamine detection in an *in vitro* setting (Peeters et al., 2013).

2. Materials and methods

2.1. Preparation and characterization of MIP-functionalized electrodes

The MIP receptors were synthesized by UV-induced bulk polymerization from acrylic acid monomers in the presence of template histamine by using EGDM (ethylene glycol dimethacrylate) as cross-linker monomer and DMSO (dimethyl sulfoxide) as porogen. All chemicals, having a purity of 99%, were purchased from Acros (Loughborough, United Kingdom). The full synthesis protocol for the MIPs used in our present work, together with their full characterization and cross-selectivity tests (against serotonin, nicotine, betahistine and histidine) are given in the reference (Peeters et al., 2013). After polymerization, the bulk polymer was ground to micro-particles and sieved with a mesh size <25 μm. The template molecules were removed by Soxhlet extraction with organic solvents and finally the particles were dried under vacuum. Non-imprinted polymer particles (NIPs) as reference material were similarly synthesized, however without adding template molecules to the polymerization suspension. The choice for acrylic acid was based on the fact that it can be deprotonated in the pH range of intestinal fluids and has therefore the ability to effectively measure histamine levels (Fujiwara et al., 1997; Peeters et al., 2013). The binding probability for histamine molecules is uniform in a pH range from 5 to 9, where they are mostly present in their single- or double-protonated state (Peeters et al., 2013). This way, the MIP material is well adjusted to cope with the physiological pH range of intestinal fluids (5.4–7.5), while histamine binding remains possible down to ≈ pH 4, albeit with decreasing affinity. Furthermore, these acrylic-acid MIPs have a negligible affinity for histidine and betahistine, molecules with similar size, shape and

functionality as histamine (Peeters et al., 2013).

The sensing electrodes, to be coated with the MIP micro-powders, consisted of titanium wires with 0.8 mm diameter, purchased from Merck Chemicals (Overijse, Belgium). Titanium was selected due to its dense, native oxide skin with a typical thickness of 3–7 nm, which makes it corrosion resistant in a wide range of pH and ionic strength. Moreover, it is an established implant material due to its biocompatibility (Wang et al., 2016; Williams, 2001). Prior to functionalization, the 3 cm long titanium electrodes were connected to flexible, insulated copper wires by spot-welding using a Soudax SD100 device (Soudax, Épône, France), see Fig. 1 for the workflow of electrode preparation. The weld joint between titanium and copper was protected with heat-shrink tubing, leaving 3 mm of the electrodes free for coating with the MIP powder after an intermediate cleaning with acetone and isopropanol. To attach the MIP powders, a viscous adhesive layer (approximately 10 μm thick) consisting of 50 mg polystyrene (molecular weight 918 kDa), Polymer Source Inc. Montreal, Canada) dissolved in 1 mL of chromatography-grade toluene (Merck Chemicals, Overijse, Belgium) was used. The Ti wires were first dipped into this solution and then, while still wet, into the MIP- or NIP powders. After curing at 130 °C inside an oven for 2 h to evaporate the toluene solvent, the electrodes were washed vigorously with MilliQ water to remove any loosely bound particles from their surface. As shown in Fig. 1a, the MIP micro-particles formed a dense layer (thickness approximately 20–30 μm) on the Ti wires. A similar approach was used by (Diliën et al., 2017) to functionalize thermocouples.

Prior to measurements inside the actual catheter, the performance of these MIP- and NIP electrodes was assessed by impedance spectroscopy. To this end, the electrodes were grouped into pairs and their functionalized side was then immersed into standard 1 mL cuvettes containing histamine spiked 1 × PBS (phosphate buffered saline) buffer. An Alpha analyzer (Novocontrol Technologies, Montabaur, Germany) in the frequency range between 60 Hz and 10 MHz at 65 mV excitation voltage under open circuit conditions was used for impedance analysis. The chosen voltage amplitude corresponds to the maximum allowed voltage for intra-body applications that do not cause unwanted cell depolarisation (Frey et al., 2010). As mentioned above, all impedance measurements were performed in non-Faradaic circumstances, i.e. without redox mediators in the liquid, since the use of such chemicals is evidently excluded when eventually doing patient studies.

2.2. Design and construction of the catheter

As a proof-of-concept, we have designed a catheter featuring the MIP-functionalized titanium electrodes at its distal end, as shown in the construction drawing in Fig. 2a. Due to ethical restrictions, this prototype was not yet tested on humans or laboratory animals, but instead in a setup that mimics the conditions inside the human intestinal tract which was filled with bowel fluids obtained from patients, see Fig. 2b.

The catheter has a total length of 200 cm, which complies with the typical lengths of naso/gastro-intestinal catheters for adults, such as those distributed by commercial manufacturers. The outer diameter is 5 mm, being the suitable for inserting a catheter through the nose, which is the established entry point for catheters probing the gastro-intestinal tract (Ang et al., 2018; Wilmer et al., 1998; Van Avestaat et al., 2016).

The catheter is constructed using a silicone rubber tube (4 mm inner- and 5 mm outer diameter, Hilltop Products, Golborne, United Kingdom) with the proximal end featuring four DuPont solderless connectors for connecting the sensing electrodes to the impedance analyzer. The electrodes are linked to these proximal connectors using four insulated copper wires that are twisted in pairs and coiled around a central aspiration tube. This configuration increases the bending stiffness of the catheter. The aspiration tube itself consists of medical-grade silicone with 1 mm outer- and 0.5 mm inner diameter (Hilltop Products, Golborne, United Kingdom). To increase the bending stiffness even further, the hollow space between the outer tube and the aspiration tube can be filled with PDMS (poly-dimethyl siloxane) rubber. In our concept experiment, this was only done for the distal part of the catheter, as shown in the construction drawing in Fig. 2a.

The distal end hosts the sample chamber with an inner volume of 100 μL and four titanium-wire electrodes; two of these are covered with a MIP layer while the other two are coated with NIP material, see Fig. 1 to view the coated electrodes mounted inside the catheter tip. The electrodes are fixated pairwise around the aspiration tube using a PEEK centering piece (PEEK: polyether ether ketone). The centering piece and the hollow space containing the electrical connections are sealed with PDMS to prevent electrical shortcuts and inflow of the liquid under test. The PDMS filling can be accomplished with a vacuum pump to pull the viscous PDMS towards the proximal end of the catheter before curing overnight at 70 °C. The intestinal liquid enters the sample chamber via an inlet featuring a polyethylene filter pad which blocks 99.5% of

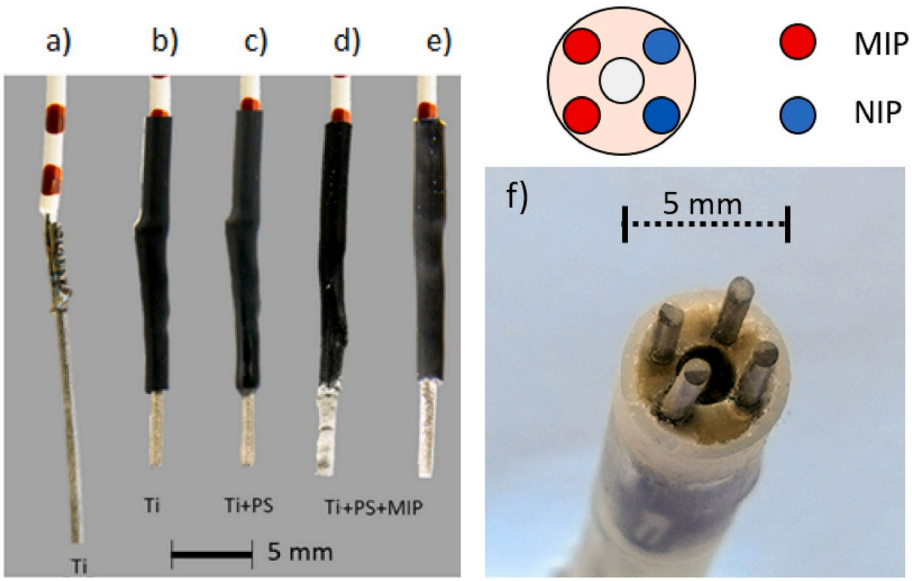

Fig. 1. Workflow of the electrode preparation with **a)** a titanium wire spot-welded to copper, **b)** with heat-shrink tube to protect the joint, **c)** after coverage with liquid polystyrene, **d)** after rolling in a MIP micro-powder and curing, and **e)** after washing off loosely bound MIP particles. **f)** Titanium electrodes in a prototype catheter with the position of the MIP and NIP pairs indicated.

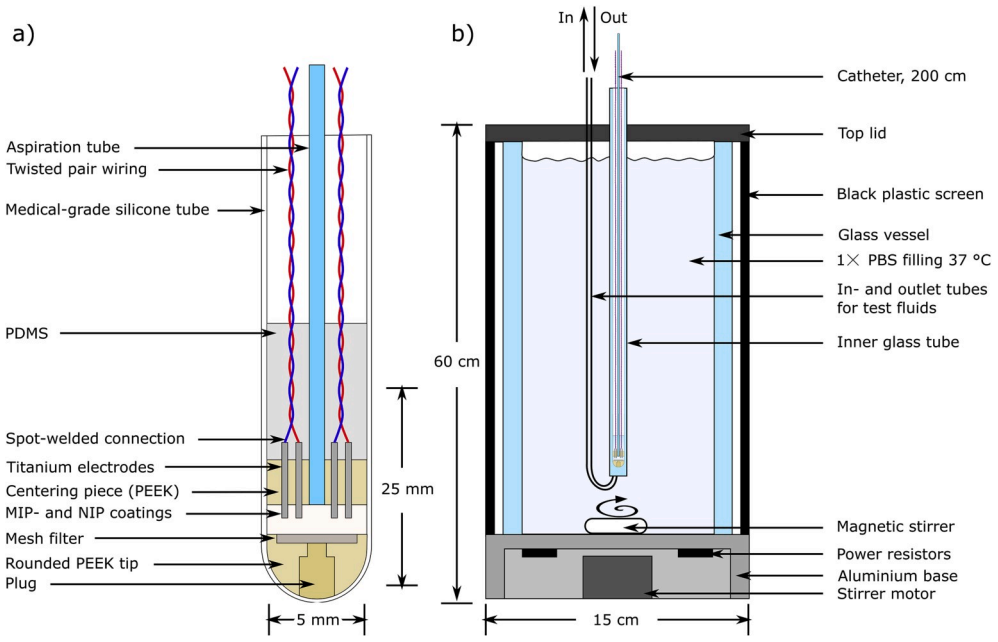

Fig. 2. a): Schematic representation of the catheter used. A medical grade silicone tube is capped off with a PEEK (polyether ether ketone) polymer block, which holds the MIP- and NIP-functionalized titanium electrodes and the aspiration tube in place. To gain stiffness and to fixate all components, the bottom section of the catheter is filled with PDMS silicone rubber. A removable plug shields the electrodes from the environment during its passage through nose, esophagus and stomach into the duodenum of a patient. See also the video in the Supporting Information. Fig. 2**b)**: Catheter-testing setup consisting of a narrow glass tube, mimicking the duodenum, which is placed centrally in a vessel that is filled with 1 × PBS buffer solution kept at a body-like temperature of 37 °C. The catheter enters the central tube from the top while liquids under study (e.g. intestinal fluids) are intruduced into the central glass tube from underneath via silicone tubing. The inner tube is removable to allow for easy decontamination in an autoclave. The bottom structure hosts heating elements and a magnetic stirrer while the entire setup is shielded against light and heat loss.

particles larger than 0.5 μm (VWR international BVBA, Leuven, Belgium). This way, solid particles that are present in a real intestinal environment cannot enter the catheter's interior. Pulling the liquid inside the sample chamber is achieved by a applying light negative pressure inside the proximal end of the aspiration tube.

Before entering the duodenum, the catheter needs to pass the stomach and stomach acids can degrade the MIP- and NIP-materials as well as the polystyrene adhesive by hydrolysis (Katzka et al., 1998). To solve this, the distal end is closed with a rounded, PEEK cap that features an integrated plug. After passing the stomach, and while being in the duodenum, the plug can first be removed by applying a positive pressure inside the aspiration tube before filling the sample chamber using suction by applying a negative pressure. A demonstration of this "blow-out & suck-in mechanism" is rendered in a video which is available in the Supporting Information. In this video, we used green-colored water instead of the pale-yellowish intestinal fluid for better visibility.

2.3. Design of the catheter testing system

In order to evaluate the performance of the gastro-intestinal catheter under body-like conditions, mimicking the circumstances inside the duodenum, we developed the testing platform shown schematically in Fig. 2b. The catheter is inserted from the top into a narrow, central glass tube with 40 cm length, 8 mm outer diameter and 6 mm inner diameter. This length corresponds roughly to the distance that a catheter has to travel from the nose of a patient to the upper part of the duodenum. Liquids under study, such as histamine-spiked buffer solutions and intestinal fluids, were administered or exchanged using two silicone tubes (inner ⌀ 1 mm, outer ⌀ 2 mm) that enter the central tube from the bottom. This allows the volume of the test liquids to be minimized to around 4 mL, resulting in a fill height of 13 cm inside this inner tube with the catheter being in place. This way, the tip of the catheter was fully immersed in fluid while the distance between the actual electrodes and the bottom of the tube was still only a few millimeters.

This inner tube was located centrally in a glass vessel (40 cm height, 9.5 cm inner diameter), filled with 1 × PBS up to 1 cm underneath its brim. The PBS filling simulates the conductive and dielectric properties of body liquids and tissues, which needs to be considered in any application involving long electrical wires loaded with an alternating voltage where the wires themselves can act (parasitically) as antennas. We kept the PBS-filled vessel, and hence the inner glass tube, at 37 °C ± 0.1 °C during all measurements using a homemade PID controller (proportional–integral–differential) with settings P = 1, I = 8, and D = 1. The temperature was monitored by two type-K thermocouples (TC-direct, Nederweert, the Netherlands), one inside the PBS filling and the other inside the inner tube, positioned at the same height as the catheter tip. The heating power was provided by eight power resistors embedded in the aluminum bottom structure underneath the glass vessel which can be regulated by the PID controller to keep the temperature at a constant 37.0 ± 0.1 °C. The bottom structure also features an integrated electromotor to drive a magnetic stirrer inside the outer glass vessel to induce fluid movement in order to obtain a homogeneous temperature distribution throughout the vessel. Furthermore, a PVC lid on top of the outer vessel holds the inner tube in place while a black plastic screen surrounds the entire platform. The latter absorbs light from the ambient thus reducing the heating power required to keep the inner parts of the platform at 37 °C; in thermal equilibrium this heating power is around 40 Watt for an ambient temperature of 20 °C.

2.4. Experimental (materials and methods)

2.4.1. Preparation of reference liquids and patients' samples

In order to study the impedimetric dose-response behavior of the MIP- and NIP-functionalized titanium electrodes, we started with a 1 × PBS solution spiked with known quantities of either histamine or histidine. Histamine was used in the form of its salt histamine dihydrochloride with a purity of at least 98% (purchased from Alfa Aesar, Karlruhe, Germany) and the resulting concentrations ranged from 2.5 nM up to 10 mM. The powder was dissolved in 1 × PBS at room temperature to create a 100 mM stock solution from which the lower concentrations were obtained by successive dilution steps. Dilutions that were not used immediately for measurements were stored in airtight containers at −21 °C in a freezer to ensure stability of the liquids. For comparison, the physiological concentration range of histamine in intestinal fluids is in the order of a few nanomolar, while for IBS patients average values up to 2 μM are documented in literature (Barbara et al., 2014; Buhner et al., 2009; Horemans et al., 2010). The histidine solutions, used to assess the cross sensitivity of the MIPs towards the parent compound histamine, were prepared similarly by dissolving pure histidine powder (>98% pure, purchased from Alfa Aesar, Germany) in 1 ×

PBS, with resulting concentrations from 10 nM up to 10 mM.

For detecting histamine in its natural matrix of bowel fluids, Maastricht University Medical Center and the University Hospital Gasthuisberg of KU Leuven provided the intestinal fluids, which were aspirated from the duodenum of healthy volunteers and from patients. The procedure in the university hospital of Leuven was approved by the Leuven University Hospitals Ethics Committee (s56910; December 18, 2015). The procedure for obtaining intestinal fluid samples from healthy volunteers in the university hospital of Maastricht was approved by the Medical Ethics Committee of the Maastricht University Medical Center, and performed in accordance with the Declaration of Helsinki (latest amendment by the World Medical Association in 2013) and the Dutch Regulations on Medical Research involving Human Subjects (WMO, 1998). This sampling procedure was part of a larger study which has been registered in the US National Library of Medicine (www.clinicaltrials.gov, ID NCT02018900). After aspiration, we mixed the bowel fluids of several individuals (three or more persons) to obtain a fluid sample with "typical" properties, which was then kept frozen at −21 °C until the start of the actual experiments. After thawing, the fluids were centrifuged (7500 rpm, 10 min, 7245 g), turning their color from opaque to a transparent yellowish tint, and the pH value was measured for which we found slight variations between pH 6 and pH 7. One sample had a pH value of 3, which is not useable for our measurements as the MIPs only bind their target down to pH 4. This was however isolated to a single patient and likely this sample contained mainly stomach fluid and only little intestinal fluid.

At this point, the bowel fluids still contained the native histamine from the patients in unknown concentrations, which is evidently not a good starting point to establish dose-response curves. Therefore, we applied a previously developed extraction protocol (Peeters et al., 2013). In short, 3 mL of bowel fluid was mixed with 10 mg of the histamine-MIP powder, and left to interact for 30 min at room temperature under constant agitation on a shaker. After that, the mixture was centrifuged (7500 rpm, 5 min, 7245 g) and the MIP particles, now loaded with the patients' histamine, were discarded. The histamine-free intestinal fluids were finally mixed with 10 vol % 1 × PBS, and subsequently spiked with appropriate amounts of histamine. This way, the patients' samples obtained their resulting, absolute histamine concentrations in the range from 2.5 nM to 0.5 mM.

3. Results and discussion

3.1. In-vitro experiments on electrode configurations

Prior to the catheter-based experiments inside the testing setup shown in Fig. 2b, we studied several electrode combinations to determine which configuration would result in the clearest correlation between a given histamine concentration and the corresponding increase of the impedance signal. These measurements were performed at room temperature in vials filled with successively increasing histamine concentrations in 1 × PBS. Due to their identical wire shape, there is no visual distinction between working- and counter electrode. We tested the following electrode couples:

i) A MIP-coated electrode and a blank Ti wire with respect to their response to histamine;
ii) Two MIP-coated electrodes and their response to histamine;
iii) Two MIP-coated electrodes and their response to histidine as a cross-sensitivity test;
iv) Two NIP-coated electrodes as a test for non-specific response to histamine.

Contrary to earlier work on impedimetric histamine detection with planar, MIP-coated working electrodes (Peeters et al., 2013), it was not possible to construct meaningful dose-response curves by plotting the impedance amplitude as a function of the histamine concentration for a single, well-chosen frequency. Instead, we utilized the entire impedance spectrum (from 60 Hz to 1 MHz) to extract the resistive component R_e of the electrode couples by fitting the data to an equivalent-circuit model. This model with four elements, of which R_e is the most important, will be described in detail in Section 3.2 and it will also serve to analyse the actual catheter measurements in Section 3.3.

As shown in Fig. 3a), the combination of a MIP-coated wire electrode with a blank titanium wire results in a meaningful dose-response curve and the concentration dependent fit (red line) was calculated based on the sigmoid dose-response model, which we address in Section 3.2. However, the resulting standard deviation was much too high and its main contributions come from the low-frequency part (below 1 kHz), where the total impedance signal is dominated by the double-layer capacity of the titanium-liquid interface. The symmetrical electrode configuration with two MIP-coated Ti wires shown in Fig. 3b) is a substantial improvement as it reduces the error margins on the correlation between the histamine concentration and the electrode resistance R_e. Therefore, we will utilize a MIP-MIP electrode couple as the active channel in the catheter-based measurements discussed in Section 3.3. Such functionalized symmetrical electrodes for MIP-based histamine detection are already known from literature in the form of dual planar electrodes, which are conceptually related to interdigitated electrodes (Bongaers et al., 2010). Furthermore, panel 3c) shows that a MIP-MIP electrode pair shows no response to histidine, which is the precursor substance of histamine and its most important competitor for binding on the MIP receptors. The final test, presented in Fig. 3d), illustrates that a NIP–NIP electrode pair does not respond to histamine, which makes it well suited as a passive reference channel for the catheter-based histamine measurements (see Section 3.3).

3.2. Data analysis of concentration-dependent impedance spectra

As mentioned above, it is hard to pinpoint a specific frequency for which the analyte concentration and the impedance data show a perfectly systematic correlation as was done in earlier publications with planar electrodes (Peeters et al., 2012, 2013; Thoelen et al., 2008). This holds not only for the experiments on histamine-spiked buffer in vials, but also for the catheter measurements: therefore, we analyzed the information contained in the integral spectrum from 60 Hz to 1 MHz by using the equivalent-circuit model shown in Fig. 4a. This circuit renders the experimental data correctly ($R^2 > 0.97$) as seen in the Bode plot (Fig. 4b) and the Nyquist representation (Fig. 4c) after a correction for the cable capacitance via a dry "air" measurement. The underlying data set was obtained with the catheter placed in the testing device kept at 37 °C, using two MIP-coated electrodes and intestinal fluid. Three concentrations were analyzed: the as prepared histamine-free fluid, and with the fluid being spiked to resulting histamine concentrations of 100 nM and 1000 nM. These values were chosen deliberately to be below, within, and above the physiologically normal concentration range.

The equivalent circuit, similar to a Randles circuit, represents the MIP layer as a resistor (R_E) and a capacitor (C_E) in parallel. Upon binding of histamine, both contributions are expected to change since MIPs are porous materials in which the histamine targets will replace water molecules in the binding pockets (Peeters et al., 2013). The circuit contains also a serial resistor R_S which comprises the Ohmic contributions of the wiring, contact resistances and the resistance of the fluid under study (see Fig. 2a). This parameter will be widely independent of the histamine concentration; however, it may decrease for the highest concentrations due to the protonating character of histamine. The three-element circuit agrees approximately with the data, however, the R^2 parameter stays around 0.85 with clear deviations in the Nyquist plots. Therefore, we added a Warburg element A_W in series to the circuit, increasing R^2 to 0.97 or higher. This element represents diffusion of charged proteins, enzymes and other molecules. A physical interpretation of the diffusion-controlled Warburg element might be seen in the fact that histamine molecules occur in three different hydrogenation

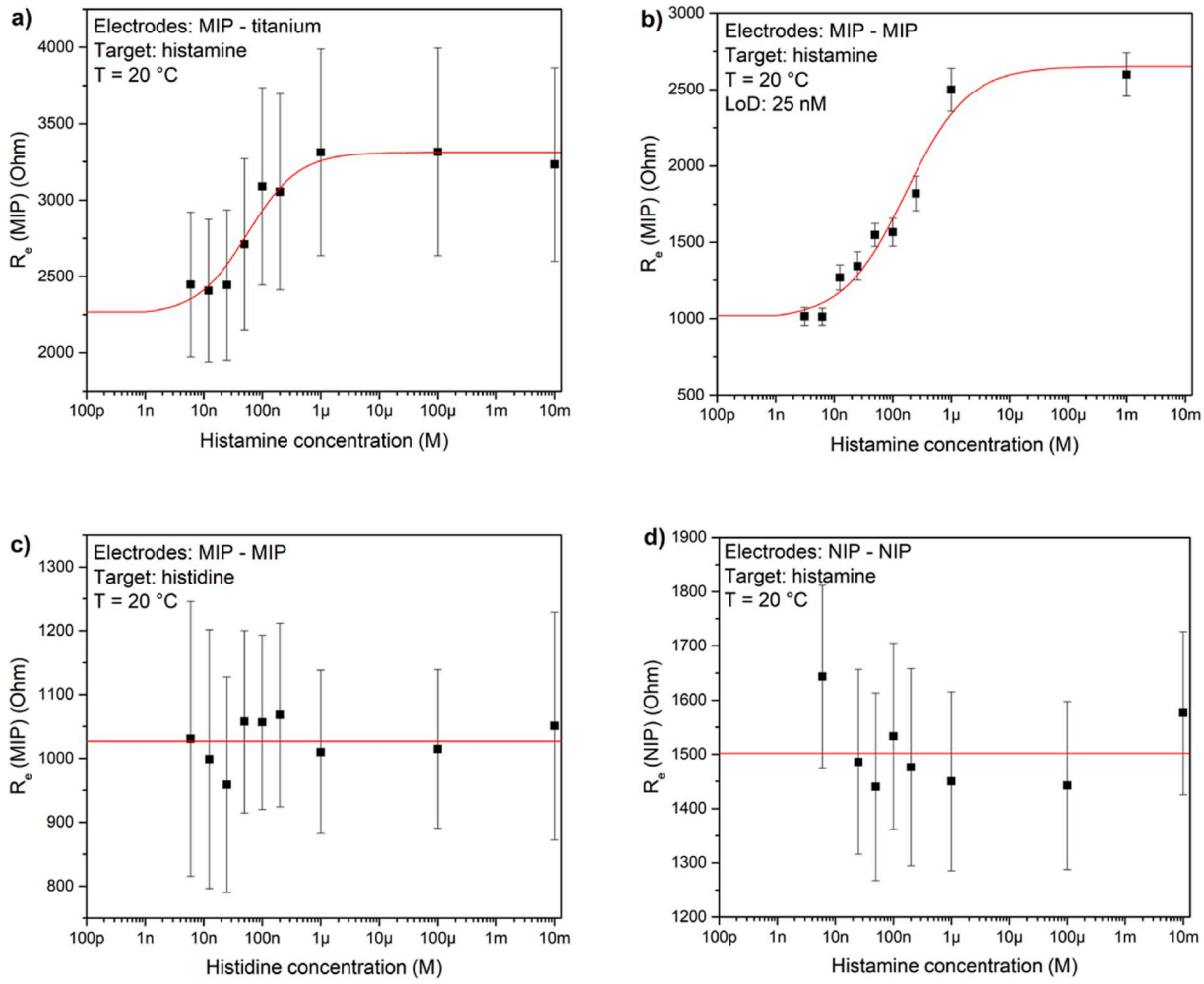

Fig. 3. Electrode resistance R_e as determined from the equivalent-circuit model of Equ. 1 for histamine- and histidine concentrations ranging from 5 nM to 10 mM in 1 × PBS buffer. All measurements were performed *in vitro* at room temperature with wire-shaped electrodes, for calculating the height of the error bars we refer to Section 3.2. Panel **a)**: The combination of a MIP-coated electrode with a blank titanium electrode shows an S-shaped response curve but with unacceptably high error margins. Panel **b)** displays the symmetrical situation with two MIP-coated wire electrodes with a detection limit of 25 nM and reduced error margins. The dose response fit line is derived using a sigmoid dose response curve (Equ. 2) for which χ^2 was minimized. As shown in panel **c)**, the combination of two MIP electrodes does not respond to the competitor histidine. According to **d)**, pairs of NIP-coated electrodes do not respond to histamine, making them suitable as a reference channel.

states that can be altered through contact with the electrodes (Chulkin and Data, 2018; Randviir and Banks, 2013).

Using these four different elements (A_W, R_E, C_E, and R_S), the frequency dependence of the complex impedance signal $Z_{tot}(\omega)$ is calculated using the following equation:

$$Z_{tot}(\omega) = \left(j\omega C_E + \frac{1}{R_E}\right)^{-1} + \frac{A_w(1-j)}{\sqrt{\omega}} + R_S \quad (1)$$

Here, ω stands for the frequency (f) while j is the imaginary unit. As seen in Fig. 4b and c, there is a good agreement between the fit function and the data. The concentration dependence of the fit parameters will be addressed in detail in Section 3.3, also including data for additional histamine concentrations. Furthermore, the full-spectrum analysis makes the data more robust with respect to electromagnetic noise that can be picked up by the cables. Regarding statistics, we wish to point out that including the entire frequency spectrum provides more reliability than considering only the impedance values at a single, fixed frequency. The error margin on fitting parameters is dictated by non-linear regression and increases with the number of fitting parameters. To this end, the model only includes four elements and omits non-essential elements such as the liquid capacitance and the double layer capacitance. We have reduced the margin of error further by measuring the same concentration at least three times and using this larger dataset to acquire more accurate dose-response curves.

The model of Equ 1. does not take into account the possibility of additional resistive and capacitive contributions due to electrode fouling, an effect that can be expected for measurements in patients' liquids. However, such influences can also be corrected by measuring differentially with an active channel (two MIP-coated electrodes) and a reference channel (two NIP-coated electrodes). The differential signal represents the intrinsic analyte concentration and this strategy was utilized successfully in earlier work on MIP-based biodetection in body fluids (Bongaers et al., 2010; Peeters et al., 2013; Thoelen et al., 2008).

3.3. Dose-response behavior of catheter measurements in testing device

In this section, we discuss the dose-response characteristics obtained with the catheter inside the testing device (kept at 37.0 ± 0.1 °C) and being filled with histamine-spiked intestinal liquids (pH 6–7). As mentioned above, these samples are mixtures obtained from several patients that we spiked with specific histamine concentrations after extraction of the native histamine. The measurements were done in

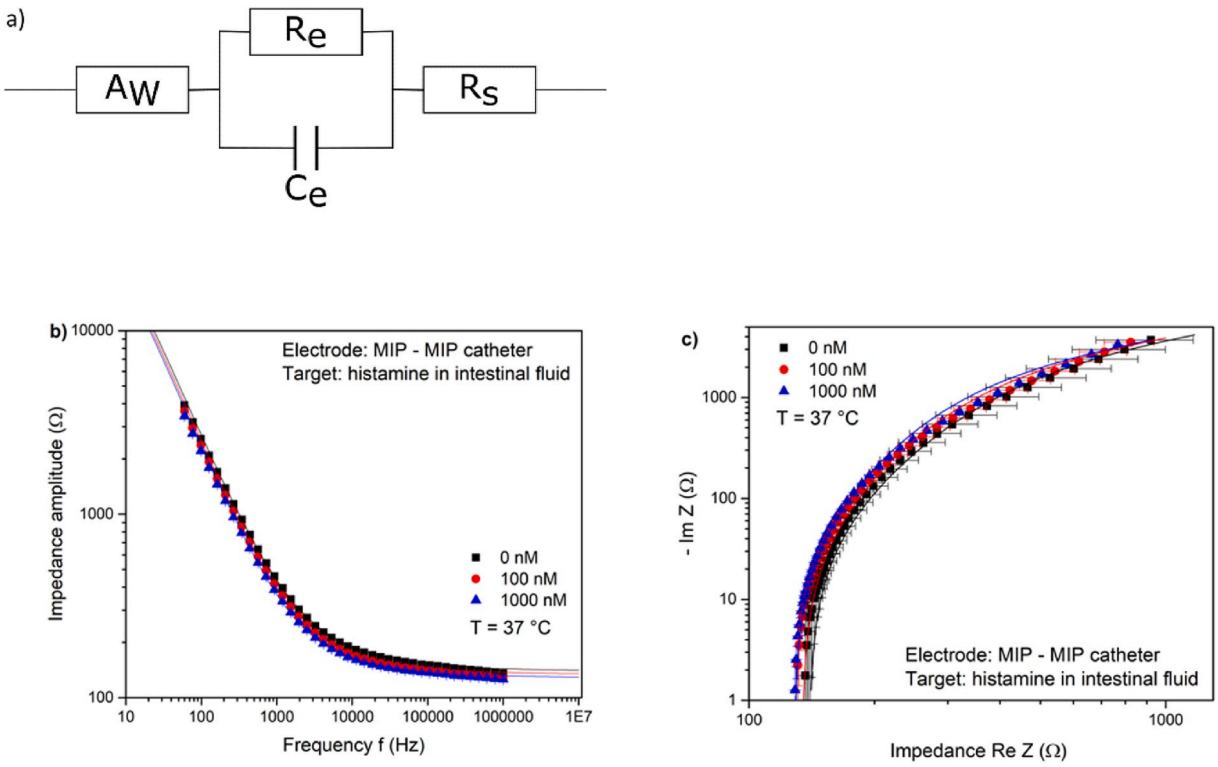

Fig. 4. a): Equivalent electric circuit for modelling the impedance spectra for different histamine concentrations in intestinal fluid, both in the in-vitro- and in the catheter-based setting. The electrode couple is presented by a resistor R_e and a capacitor C_E in parallel, the Warburg element stands for diffusion of charged molecules and the resistor R_S comprises the cable- and fluid resistance. Panel **b)** shows the associated fit to the data in Bode representation (using Equ. 1) for histamine-free bowel fluid and for bowel fluid with 100 nM, and 1000 nM histamine. **c)** Nyquist representation of the data with fitting derived from the model of panel 4**a)**, illustrating the quality of the equivalent-circuit model with $R^2 > 0.99$.

increasing order of the spiked concentration, starting from histamine-free fluid, without regeneration of the electrodes between measurements. Fig. 5a shows the concentration dependence of the electrode-resistance parameter R_E. Within the relevant range for healthy persons, from 5 nM up to 200 nM, the response is linear with respect to the logarithm of the concentration and corresponds to ≈6 kΩ/log c (6 kΩ per decade). The scaling proportional to the logarithm of the concentration can supposedly be explained by the fact that histamine molecules are positively charged, a behavior that is similarly observed in the pH-dependent surface potential of many oxides such as Ta_2O_2 (Poghossian et al., 2018). The highest sensitivity $\Delta R_e/\Delta c \approx 209$ Ω/nM was found in the concentration regime around 16 nM, which is within the

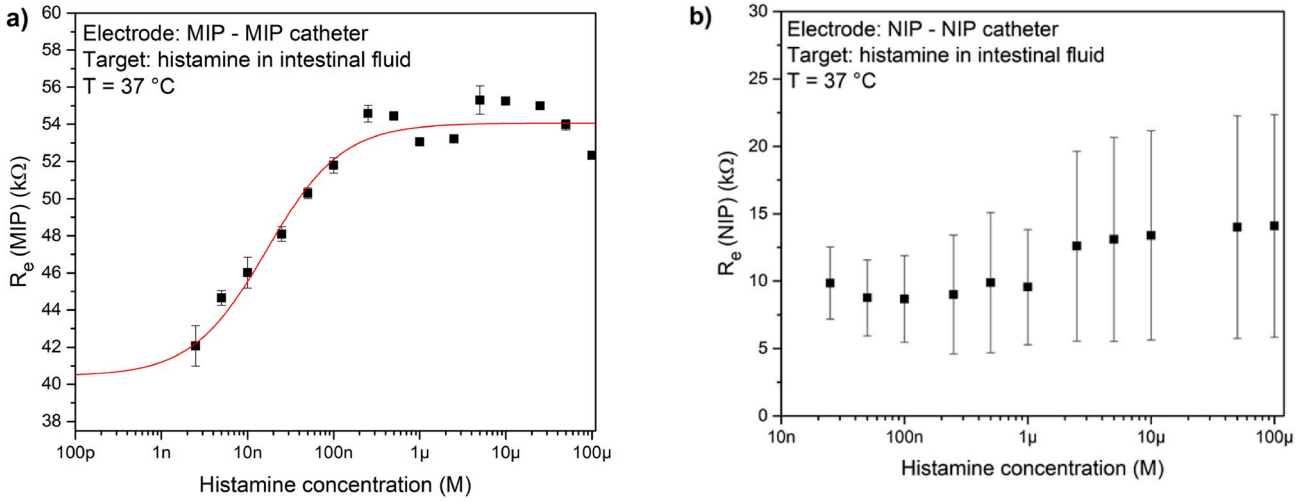

Fig. 5. Dose-response behavior of the electrode-resistance parameter R_e, measured with the histamine-sensing catheter on intestinal fluids in the catheter-testing device (at 37 °C). The left panel **a)** refers to the MIP-MIP electrode couple, following nicely the binding model of Equ. 2, which is indicated by a solid red line. Error bars, if not shown, are smaller than symbol size. The right panel **b)** are the results for the NIP–NIP reference channel with only a weak response to increasing histamine concentration. All data points are the averages of four consecutive full-spectrum measurements while the error bars represent the standard deviations. In between subsequent concentrations, there was no electrode regeneration. (For interpretation of the references to color in this figure legend, the reader is referred to the Web version of this article.)

diagnostically relevant range. All data points are the averages obtained from four subsequent measurements of the entire spectrum from 60 Hz to 1 MHz, meaning that measuring a given concentration takes 120 s (four cycles of 30 s). The spectra were analyzed with Equ. 1, based on the equivalent-circuit model shown in Fig. 4a. The corresponding data for the NIP–NIP electrode couple are given in Fig. 5b, showing a non-systematic response which is lower and occurs only far above the physiological concentration range.

The dose-response behavior of the MIP-MIP signal follows the sigmoid dose response curve, which is given in Equ. 2 and was implemented in the Matlab 2018b software package and exported to Origin pro 2016 for the graphical layout of the fit-function (Cornelis et al., 2018; Yadav, 2013).

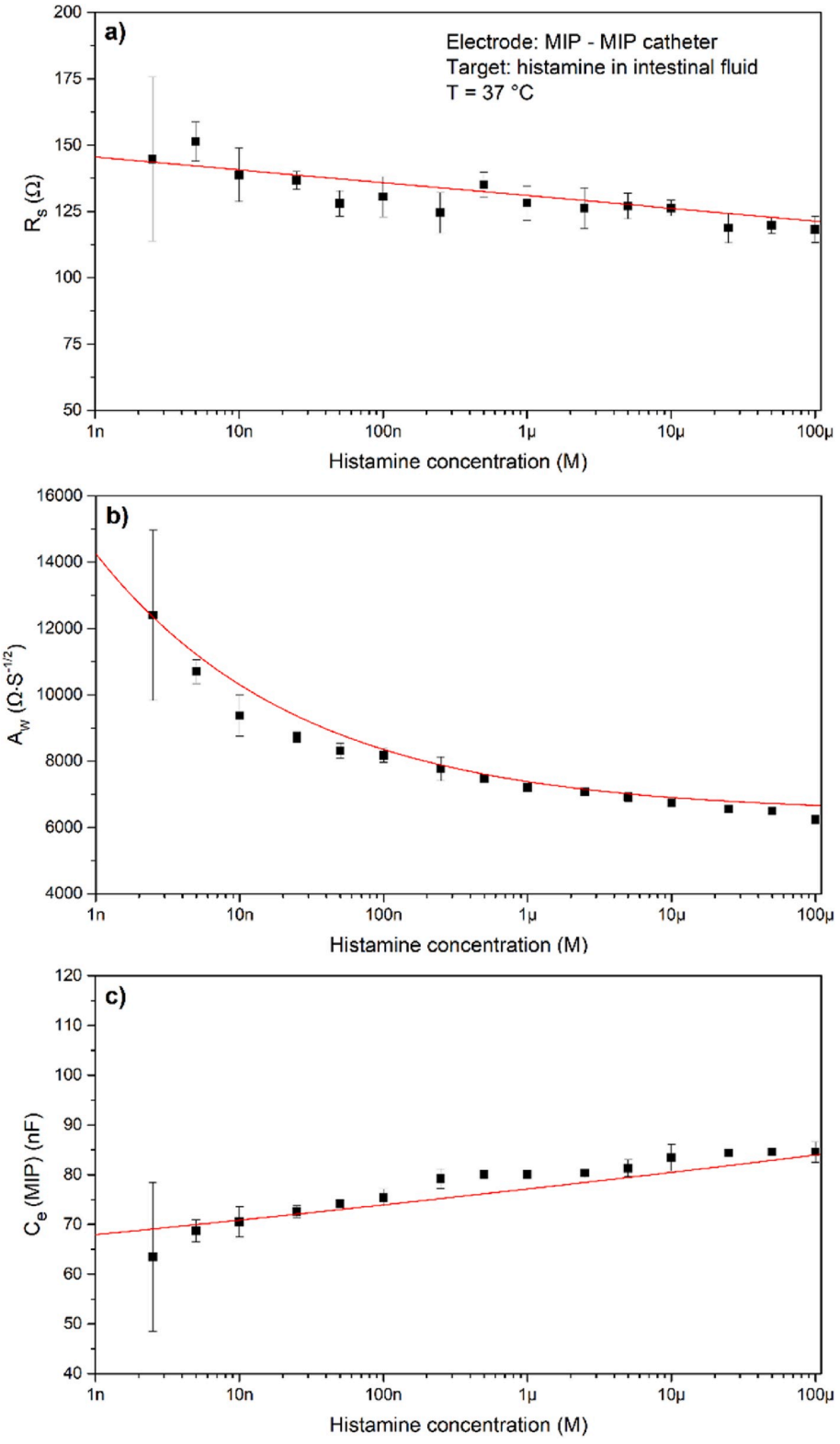

Fig. 6. Concentration dependence of the solution resistance R_s **(a)**, the Warburg element A_W **(b)** and the electrode capacity C_E **(c)** of the MIP-MIP electrode couple according to the equivalent-circuit model of Fig. 4a. R_s and A_W show a minor decrease, supposedly due to the weakly acidic behavior of the spiked histamine and possible transitions between its protonation states. The capacity signal displays similarities with electrode resistance R_e, however the sensitivity is not as pronounced in the diagnostically relevant concentration regime.

$$R(C) = \mathrm{R_{min}} + \frac{(R_{max} - R_{min})}{\left(1 + 10^{((\ (\ \log10(D50) - \log10(C)\ )*\mathrm{Slope}\ )\ )}\right)} \quad (2)$$

The fit parameters of the sigmoid response model are $R_{min} = 40.4\ k\Omega$, $R_{max} = 54\ k\Omega$, slope = 1 and $d_{50} = 16$ nM, resulting in a goodness factor $R^2 = 0.91$. The linear range is approximately between 5 nM and 200 nM, corresponding to physiologically normal histamine values in duodenum fluid while typical concentrations found with IBS patients are 1–2 μM, thus in the saturation regime of the sensor (Peeters et al., 2013). In a real application, the software can therefore be configured to provide digital information between subcritical (negative result if c < 200 nM) and critical values (positive result if c > 200 nM). IBS patients, in whom mast cell activation with histamine release is the underlying pathophysiological mechanism, should fall into the second category, when appropriately challenged with a food or a stressor (Fritscher-Ravens et al., 2019; Vanuytsel et al., 2014). The relative signal value upon saturation (141%) agrees well with the signal amplitudes found earlier for MIP-based impedimetric sensors for the detection of L-nicotine and histamine (Bongaers et al., 2010; Thoelen et al., 2008). In one measurement (data not shown), the intestinal fluid was heavily contaminated with stomach acid, resulting in a pH of 3. Here, it was not possible to construct a dose-response curve, which can actually be anticipated from the pH-dependend binding properties of the MIP coating. The poly (acrylic acid) MIPs have a uniform binding affinity between pH 5 and pH 9, while the affinity drops rapidly to zero outside this range: At pH 3 the affinity is less than 10% compared to pH 6–7 (Peeters et al., 2013). Fig. 6 summarizes the concentration dependence of the other three parameters as derived from the equivalent-circuit model introduced in Fig. 4a, being the capacitance C_e of the electrodes, the Warburg element A_W and the solution- and serial resistance R_s.

The R_s parameter shows a weak, almost linear decrease, which we can attribute to the mildly acidic character of histamine that enhances the conductivy of the liquid by release of H^+ ions. The same holds for the Warburg element in which higher ion concentrations enhance conductivity by diffusion of charged species that are protonated or deprotonated in close vicinity of the electrode. In contrast to the data for the electrode resistance R_e (see Fig. 5), A_W does not saturate for concentrations above 1 μM, which means that the A_W response is unrelated to selective molecular recognition. The electrode capacitance C_e shows a gradual increase by ca. 22% between an almost histamine-free solution (5 nM) and the saturated level. Therefore, the correlation between the spiked concentrations and C_e is weak in the relevant regime, which makes C_e much less suited as a read-out parameter than R_e.

4. Conclusions and summary

In this work, we have developed a catheter-based impedimetric sensor for the detection of histamine in intestinal fluids. In a later stage of development, this catheter should serve as a tool to facilitate the diagnosis of irritable bowel syndrome, a widespread disorder which goes along with elevated histamine levels in the small intestines due to chronic immune activation. The analytical performance was verified by measurements on histamine-spiked intestinal fluids from humans inside a testing setup that mimics body temperature and the dielectric properties of tissue and body liquids. The length and diameter of the catheter comply with the needs for insertion through the nose, although a further reduction of the outer diameter is desirable in view of the comfort of future patients on whom the device will be applied *in vivo*. Thanks to an integrated aspiration tube, intestinal liquid can also be obtained for an additional *in vitro* analysis of the fluid regarding histamine and other biomarkers. Furthermore, the aspiration tube serves to open the tip compartment with the histamine-sensitive electrodes only after its passage through the stomach: This avoids deterioration of the electrode coatings by stomach acid and allows also to open the tip compartment deliberately at any later moment.

Regarding the electrode configuration, we found the highest correlation between impedance data and the histamine concentration when using "symmetric" electrode couples in which both titanium wires were coated with MIP-receptor material. The tip compartment contains furthermore a couple of NIP-coated electrodes, allowing to correct the data for electrode fouling if necessary. To quantify the impedance response to increasing histamine levels, we analyzed the full impedance spectrum in a frequency range spanning almost 5 orders of magnitude to extract the electrode resistance: This resistance was obtained as one out of four parameters in a modified Randles circuit; the three other parameters show either a very weak concentration dependence or do not result in sufficient sensitivity within the relevant concentration range. The electrode-resistance parameter follows a sigmoid dependence on the histamine concentration and the useful analytical range is between 5 nM and 200 nM, with the highest sensitivity around 16 nM. This covers the physiologically normal range while the sensor signal saturates for concentrations above 200 nM, typical for pathological conditions.

It is a considerable challenge to develop a proof-of-concept in the laboratory further towards an envisaged application, for which the strict regulatory rules on medical devices apply. The catheter-based impedimetric histamine sensor is now at a technological-readiness level that tests on laboratory animals and, in a following stage, on human volunteers become feasible. Along with this, further refinements are under consideration aiming at i) a narrowing down of the external catheter diameter by using MIP-functionalized microelectrodes and ii) utilizing MIP-deposition techniques that can be upscaled towards mass production.

Declaration of competing interest

The authors declare that they have no known competing financial interests or personal relationships that could have appeared to influence the work reported in this paper.

CRediT authorship contribution statement

Gideon Wackers: Validation, Formal analysis, Investigation, Writing - original draft, Writing - review & editing, Visualization. **Tristan Putzeys:** Methodology, Software, Validation, Formal analysis, Writing - original draft. **Marloes Peeters:** Conceptualization, Methodology, Writing - original draft, Resources. **Lori Van de Cauter:** Validation, Investigation. **Peter Cornelis:** Software, Resources, Data curation. **Michael Wübbenhorst:** Resources, Supervision. **Jan Tack:** Resources, Writing - original draft, Writing - review & editing. **Freddy Troost:** Resources, Writing - original draft, Writing - review & editing. **Nicolas Verhaert:** Supervision, Funding acquisition. **Theodor Doll:** Conceptualization, Methodology. **Patrick Wagner:** Conceptualization, Methodology, Investigation, Supervision, Writing - original draft, Writing - review & editing, Project administration, Funding acquisition.

Acknowledgments

We kindly acknowledge financial support by the Research Foundation Flanders FWO for funding the project G.0B25.14N "Monitoring of gut functions and inflammation processes with biomimetic sensors based on molecularly imprinted polymers". Tristan Putzeys acknowledges funding by Research Foundation Flanders FWO (12Y6919N). Nicolas Verhaert is partially supported by Research Foundation Flanders FWO (1804816 N). Marloes Peeters is supported by the EPSRC New Investigator Award EP/R029296/1. Partial co-funding by the German DFG Cluster of excellence 2177 Hearing4All was received through Theodor Doll. The authors also wish to thank Prof. Robert Jan Brummer from the School of Medical Sciences at Örebro University (Sweden) cordially for many stimulating discussions in the starting-up phase of the presented work. Assistance in making the demonstration video by Carlos Henrique Campos and Larissa Kim from the universidade de São Paulo (Brazil) is cordially appreciated, their Professor Jonas Gruber made their

internship at KU Leuven possible.

Appendix A. Supplementary data

Supplementary data to this article can be found online at https://doi.org/10.1016/j.bios.2020.112152.

References

Adler, S., Metzger, Y., 2011. Therap, Adv, Gastroenterol, 4 (4), 265–268.
Ang, D., Pannemans, J., Vanuytsel, T., Tack, J., 2018. Neuro Gastroenterol. Motil. 30 (9) art no. e13357.
Aygün, O., Schneider, E., Scheuer, R., Usleber, E., Gareis, M., Märtlbauer, E., 1999. J. Agric. Food Chem. 47 (5), 1961–1964.
Bandodkar, A.J., Molinnus, D., Mirza, O., Guinovart, T., Windmiller, J.R., Valdés-Ramérez, G., Andrade, F.J., Schöning, M.J., Wang, J., 2014. Biosens. Bioelectron. 54, 603–609.
Barbara, Giovanni, Cremon, Cesare, Stanghellini, Vincenzo, 2014. Curr. Opin. Gastroenterol. 30 (4), 352–358.
Barbara, G., Stanghellini, V., De Giorgio, R., Cremon, C., Cottrell, G.S., Santini, D., Pasquinelli, G., Morselli-Labate, A.M., Grady, E.F., Bunnett, N.W., Collins, S.M., Corinaldesi, R., 2004. Gastroenterology 126, 693–702.
Belon, P., Cumps, J., Ennis, M., Mannaioni, P.F., Roberfroid, M., Sainte-Laudy, J., Wiegant, F.A.C., 2004. Inflamm. Res. 53, 181–188.
Bindra, D.S., Zhang, Y., Wilson, G.S., Sternberg, R., Thévenot, D.R., Moatti, D., Reach, G., 1991. Anal. Chem. 63 (17), 1692–1696.
Bongaers, E., Alenus, J., Horemans, F., Weustenraed, A., Lutsen, L., Vanderzande, D., Cleij, T.J., Troost, F.J., Brummer, R.J., Wagner, P., 2010. Phys. Status Solidi 207 (4), 837–843.
Buhner, S., Li, Q., Vignali, S., Barbara, G., De Giorgio, R., Stanghellni, V., Cremon, C., Zeller, F., Langer, R., Daniel, H., Michel, K., Schemann, M., 2009. Gastroenterology 137 (4), 1424–1434.
Canavan, C., West, J., Card, T., 2014. Clin. Epidemiol. 6, 71–80.
Chulkin, P., Data, P., 2018. JoVE 140, 8.
Cornelis, P., Givanoudi, S., Yongabi, D., Iken, H., Duwe, S., Deschaume, O., Robbens, J., Dedecker, P., Bartic, C., Wübbenhorst, M., Schöning, M.J., Heyndrickx, M., Wagner, P., 2018. Biosens. Bioelectron. 136, 97–105.
Diliën, H., Peeters, M., Royakkers, J., Harings, J., Cornelis, P., Wagner, P., Redeker, E., Banks, C., Eersels, K., van Grinsven, B., Cleij, T., 2017. Sensors 2 (4), 583–589.
Dressman, J.B., Berardi, R.R., Dermentzoglou, L.C., Russell, T.L., Schmaltz, S., Barnett, J., Jarvenpaa, K., 1990. Pharmaceut. Res. 7 (7), 756–761.
Drossman, D.A., Tack, J., Ford, A.C., Szigethy, E., Törnblom, H., Van Oudenhove, L., 2018. Gastroenterology 154 (4), 1140–1171.
Frey, O., Holtzman, T., McNamara, R.M., Theobald, D.E.H., van der Wal, P.D., de Rooij, N.F., Dalley, J.W., Koudelka-Hep, M., 2010. Biosens. Bioelectron. 26 (2), 477–484.
Fritscher-Ravens, A., Pflaum, T., Mösinger, M., Ruchay, Z., Röcken, C., Milla, P.J., Das, M., Böttner, M., Wedel, T., Schuppan, D., 2019. Gastroenterology 157 (1), 109–118.
Frost, M., Meyerhoff, M.E., 2006. Anal. Chem. 78 (21), 7370–7377.
Fujiwara, M., Grubbs, R.H., Baldeschwieler, J.D., 1997. J. Colloid Interface Sci. 185 (1), 210–216.
Horemans, F., Alenus, J., Bongaers, E., Weustenraed, A., Thoelen, R., Duchateau, J., Lutsen, L., Vanderzande, D., Wagner, P., Cleij, T.J., 2010. Sensor. Actuator. B Chem. 148 (2), 392–398.
Katzka, D.A., Gideon, R.M., Castell, D.O., 1998. Am. J. Gastroenterol. 93, 1236–1242.
Kim, J., Imani, S., de Araujo, W.R., Warchall, J., Valdés-Ramírez, G., Paixão, T.R.L.C., Mercier, P.P., Wang, J., 2015. Biosens. Bioelectron. 74, 1061–1068.
Kotanen, C.N., Moussy, F.G., Carrara, S., Guiseppi-Elie, A., 2012. Biosens. Bioelectron. 35 (1), 14–26.
Li, C.Y., Wu, P.M., Han, J., Ahn, C.H., 2008. Biomed. Microdevices 10 (5), 671–679.
Li, C.Y., Ahn, C.H., Shutter, L.A., Narayan, R.K., 2009. Biosens. Bioelectron. 25 (1), 173–178.
Lobo, B, Ramos, L, Martínez, C, Guilarte, M, González-Castro, AM, Alonso-Cotoner, C, Pigrau, M, de Torres, I, Rodiño-Janeiro, BK, Salvo-Romero, E, Fortea, M, Pardo-Camacho, C, Guagnozzi, D, Azpiroz, F, Santos, J, Vicario, M, 2017. Unit. Eur. Gastroenterol. J. 5 (6), 887–897.
Loyez, M., Larrieu, J.C., Chevineau, S., Remmelink, M., Leduc, D., Bondue, B., Lambert, P., Devière, J., Wattiez, R., Caucheteur, C., 2019. Biosens. Bioelectron. 131, 104–112.
Mairal Lerga, T., Jauset-Rubio, M., Skouridou, V., Bashammakh, A.S., El-Shahawi, M.S., Alyoubi, A.O., O'Sullivan, C.K., 2019. Anal. Chem. 91 (11), 7104–7111.
Mamleyev, E.R., Heissler, S., Nefedov, A., Weidler, P.G., Nordin, N., Kudryashov, V.V., Länge, K., MacKinnon, N., Sharma, S., 2019. npj Flex. Electron. 3 (2), 11.
Mattsson, L., Xu, J., Preininger, C., Tse Sum Bui, B., Haupt, K., 2018. Talanta 181, 190–196.
Mattsson, C., Doppler, L., Preininger, S., 2017. Chemosensors 5, 33.
McCaul, M., Glennon, T., Diamond, D., 2017. Curr. Opin. Electrochem. 3 (1), 46–50.
Molinnus, D., Hardt, G., Käver, L., Willenberg, H.S., Kröger, J.-C., Poghossian, A., Keusgen, M., Schöning, M.J., 2018. Sensor. Actuator. B Chem. 272, 21–27.
Muscarella, M., Iammarinol, M., Centonze, D., Palermo, C., 2005. Vet. Res. Commun. 29 (2), 343–346.
Peeters, M., Troost, F.J., van Grinsven, B., Horemans, F., Alenus, J., Murib, M.S., Keszthelyi, D., Ethirajan, A., Thoelen, R., Cleij, T.J., Wagner, P., 2012. Sensor. Actuator. B Chem. 171–172, 602–610.
Peeters, M., Troost, F.J., Mingels, R.H.G., Welsch, T., van Grinsven, B., Vranken, T., Ingebrandt, S., Thoelen, R., Cleij, T.J., Wagner, P., 2013. Anal. Chem. 85 (3), 1475–1483.
Peeters, M., Kobben, S., Jiménez-Monroy, K.L., Modesto, L., Kraus, M., Vandenryt, T., Gaulke, A., van Grinsven, B., Ingebrandt, S., Junkers, T., Wagner, P., 2014. Sensor. Actuator. B Chem. 203, 527–535.
Pennazio, M., Spada, C., Eliakim, R., Keuchel, M., May, A., Mulder, C.J., Rondonotti, E., Adler, S., Albert, J., Baltes, P., Barbaro, F., Cellier, C., Charton, J.P., Delvaux, M., Despott, E.J., Domagk, D., Klein, A., McAlindon, M., Rosa, B., Rowse, G., Sanders, D. S., Saurin, J.C., Sidhu, R., Dumonceau, J.M., Hassan, C., Gralnek, I., 2015. Endoscopy 47 (5), 352–376.
Pickup, J.C., Hussain, F., Evans, N.D., Sachedina, N., 2005. Biosens. Bioelectron. 20 (10), 1897–1902.
Poghossian, A., Jablonski, M., Koch, C., Bronder, T.S., Rolka, D., Wege, C., Schöning, M. J., 2018. Biosens. Bioelectron. 110, 168–174.
Ramakers, G., Wackers, G., Trouillet, V., Welle, A., Wagner, P., Junkers, T., 2019. Macromolecules 52 (6), 2304–2313.
Randviir, E.P., Banks, C.E., 2013. Anal. Methods 5, 1098–1115.
Ratautaite, V., Nesladek, M., Ramanavicience, A., Baleviciute, I., Ramanavicius, A., 2014. Electroanalysis 26, 2458–2464.
Schmulson, M.J., Drossman, D.A., 2018. J. Neurogastroenterol. Motil. 23 (2), 151–163.
Tan, N.D., Gwee, K.A., Tack, J., Zhang, M.Y., Li, Y.W., Chen, M.H., Xiao, Y.L., 2019. J. Gastroenterol. Hepatol. 11. https://doi.org/10.1111/jgh.14905.
Thoelen, R., Vansweevelt, R., Duchateau, J., Horemans, F., D'Haen, J., Lutsen, L., Vanderzande, D., Ameloot, M., vandeVen, M., Cleij, T.J., Wagner, P., 2008. Biosens. Bioelectron. 23 (6), 913–918.
Torres, J., Gsponer, N., Ramírez, C.L., Vera, D., Mariano, A., Montejano, H.A., Chesta, Carlos A., 2012. J. Chromatogr. A 1266, 24–33.
Tseng, T.T.C., Monbouquette, H.G., 2012. J. Electroanal. Chem. 682, 141–146.
Van Avestaat, M., Ripken, D., Hendriks, H.F., Masclee, A.A., Troost, Fj, 2016. Int. J. Obes. 41 (2), 217–224.
Van Gossum, A., 2014. Curr. Opin. Gastroenterol. 30 (5), 472–476.
van Grinsven, B., Eersels, K., Peeters, M., Losada-Pérez, P., Vandenryt, T., Cleij, T.J., Wagner, P., 2014. ACS Appl. Mater. Interfaces 6 (16), 13309–13318.
Vanuytsel, T., van Wanrooy, S., Vanheel, H., Vanormelingen, C., Verschueren, S., Houben, E., Salim Rasoel, S., Tóth, J., Holvoet, L., Farré, R., Van Oudenhove, L., Boeckxstaens, G., Verbeke, K., Tack, J., 2014. Gut 63 (8), 1293–1299.
Wackers, G., Vandenryt, T., Cornelis, P., Kellens, E., Thoelen, R., De Ceuninck, W., Losada-Pérez, P., van Grinsven, B., Peeters, M., Wagner, P., 2014. Sensors 14 (6), 11016–11030.
Wang, G., Li, J., Lv, K., Zhang, W., Ding, X., Yang, G., Liu, X., Jiang, X., 2016. Sci. Rep. 6 (31769), 13pp.
Williams, D.F., 2001. Titanium for Medical Applications. Springer-Verlag GmbH, Berlin Heidelberg, pp. 13–24.
Wilmer, A., Van Cutsem, E., Andrioli, A., Tack, J., Coremans, G., Janssens, J., 1998. Gut 42 (2), 235–242.
Wilson, G.S., Gifford, R., 2005. Biosens. Bioelectron. 20 (12), 2388–2403.
Wood, J.D., 2006. Gut 55, 445–447.
Worning, H., Müllertz, S., 1966. Scand. J. Gastroenterol. 1 (4), 268–283.
Wouters, M.M., Balemans, D., Van Wanrooy, S., Dooley, J., Cibert-Goton, V., Alpizar, Y. A., Valdez-Morales, E.E., Nasser, Y., Van Veldhoven, P.P., Vanbrabant, W., Van der Merwe, S., Mols, R., Ghesquière, B., Cirillo, C., Kortekaas, I., Carmeliet, P., Peetermans, W.E., Vermeire, S., Rutgeerts, P., Augustijns, P., Hellings, P.W., Belmans, A., Vanner, S., Bulmer, D.C., Talavera, K., Vanden Berghe, P., Liston, A., Boeckxstaens, G.E., 2016. Gastroenterology 150 (4), 875–887.
Yadav, S.K., 2013. Int. J. Environ. Sci. Dev. Monit 4 (3), 77–80.
Yao, H.F., Shum, A.J., Cowan, M., Lähdesmäki, I., Parviz, B.A., 2011. Biosens. Bioelectron. 26 (7), 3290–3296.